THE LOCATIONS AND CHARACTERISTICS OF THE AFTERSHOCKS OF THE OCTOBER 3, 1974, PERUVIAN EARTHQUAKE

by

Charley John Langer

Thesis submitted to the Graduate Faculty of the
Virginia Polytechnic Institute and State University
in partial fulfillment of the requirements for the degree of

MASTER OF SCIENCE

in

Geophysics

APPROVED:

G. A. Bollinger, Chairman

J. K. Costain

E. S. Robinson

M. C. Gilbert

C. E. Sears

March, 1977
Blacksburg, Virginia

ACKNOWLEDGMENTS

Appreciation is extended to the Organization of American States (OAS) and to Centro Regional de Seismologia para América del Sur (CERESIS) for their aid in helping to fund this study.

Particular recognition is due to , General Director, Instituto Geofisico del Peru and to , Senior Research Geophysicist, Instituto Geofisico del Peru, for their assistance and encouragement during all phases of the field operations. Special thanks are extended to all other personnel of the IGP for helping to make this project a success.

Helpful discussions and the support of , , and were of great benefit to the investigation. and assisted with the data reduction.

, NOAA/EDS, National Geophysical and Solar-Terrestrial Data Center, provided computer time and his services in running the focal mechanism solution program.
furnished information pertaining to Peruvian earthquakes from the NOAA/EDS Earthquake Data File.

LM/MAJ 6/2/77

TABLE OF CONTENTS

INTRODUCTION

The magnitude-7.6 (M_S) Peruvian earthquake of October 3, 1974, occurred within a segment of the shallow seismic belt that bounds western South America. Earthquakes of large magnitude are not uncommon to the coastal areas of Peru (e.g., Silgado, 1968; 1973) and represent, in all probability, the ongoing process of the Nazca plate underthrusting the more stable Americas plate (Isacks *et al.*, 1968).

Prior to this study, there had been no attempt to investigate, in detail, an aftershock sequence of a major South American earthquake. The field work involved in such a task is usually difficult, if not impossible, because of the large aftershock zones and remote areas in which they occur. The earthquake of October 3, however, presented a rather unique situation. Although the main shock epicenter was oceanward, west-southwest of Lima, excellent paved highways along the coast to the northwest and southeast provided a practical means for using surface vehicles to install and maintain a temporary regional seismograph network that would essentially bracket the aftershock zone to the north and south. Also, there were three seismic observatories within the area of interest that could be used to augment a temporary network. Therefore, at the request of the Instituto Geofisico del Peru (IGP), the U.S. Geological Survey (USGS) dispatched a team of seismologists to Lima on October 5 with five portable seismograph systems. The field work for this study represents a joint effort between the IGP and the USGS, and has provided data for the location of 113 hypocenters which are considered to be a representative sample of the aftershock activity during the period of investigation.

PHYSIOGRAPHIC AND GEOLOGICAL FEATURES

Peru, the third largest country in South America, extends along the western side of the continent from near the equator to about 18.3°S latitude. It is bounded on the east principally by the Amazon basin of Brazil and to the west by southern Ecuador and the Pacific Ocean.

Within the region of study (Figure 1), three major geographic units exist: the Andes mountain system, the coastal area, and the Peru-Chile trench. The Andean system is formed from two mountain ranges referred to as the western cordillera (Cordillera Occidental) and the eastern cordillera (Cordillera Oriental), both of which are generally subparallel with the coast between northern Peru and about 12°S latitude. South of 12°S latitude they begin to branch apart; the western cordillera continues to parallel the coast whereas the eastern cordillera is deflected inland and assumes a more east-southeasterly strike. In southern Peru, the two ranges become completely separated by a high plateau termed the altiplano. The coastal area varies in width between about 20 and 75 kilometers with moderate relief ranging from sea level to over 700 meters. It is characterized by marine terraces and broad alluvial planes dissected by numerous valleys with intermittent rivers, which extend to the Andean foothills (Bellido B., 1969). The Peru-Chile trench is a narrow, deep oceanic basin which closely parallels most of the west coast of South America. It is the boundary between the converging Nazca and Americas plates and is representative of a typical island-arc trench system, i.e., it has asso-

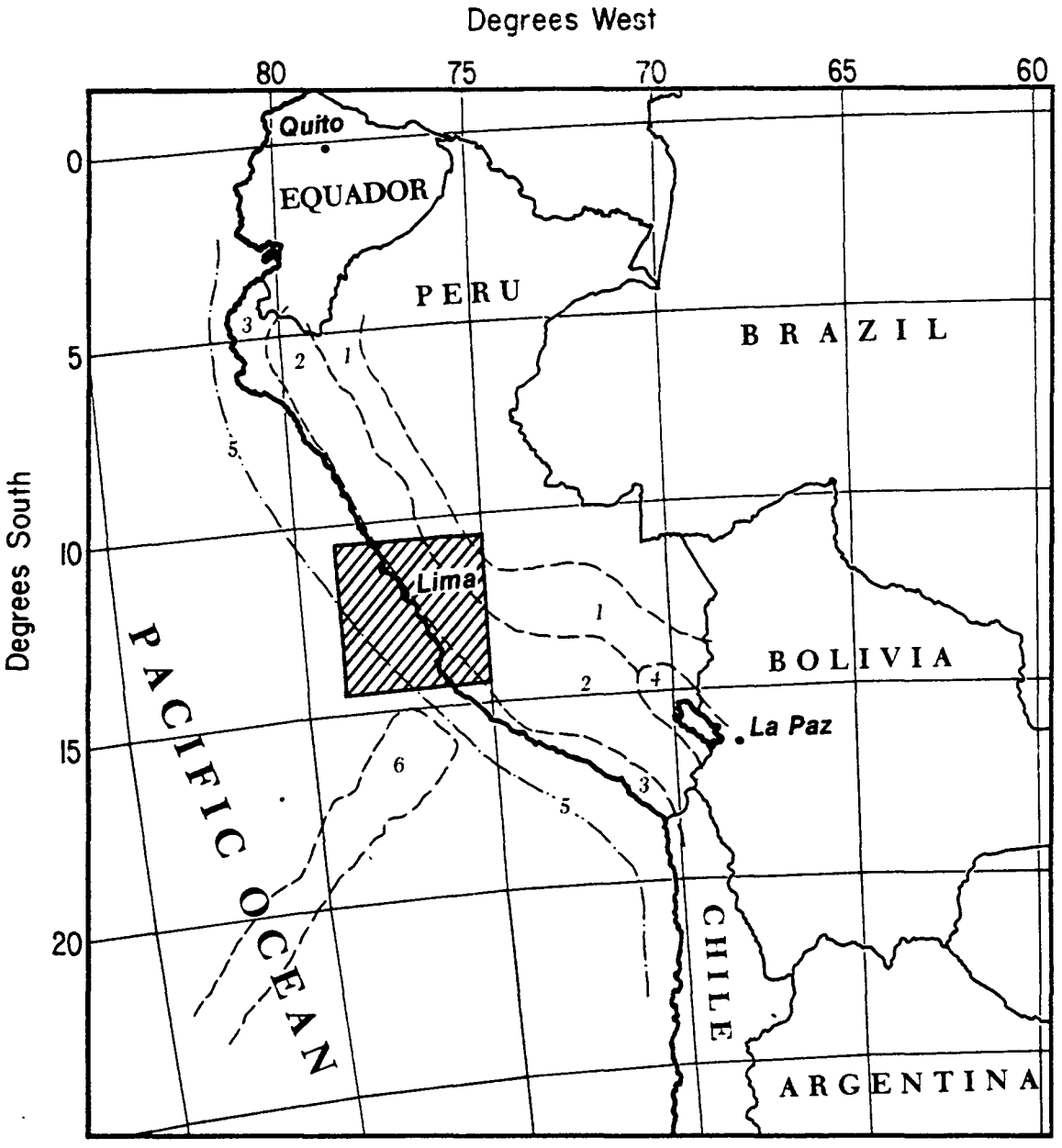

Figure 1. Location map showing area of study (cross-hatching) and major geologic and physiographic provinces: 1 - eastern cordillera, 2 - western cordillera, 3 - coastal area, 4 - altiplano, 5 - Peru-Chile trench, 6 - Nazca Ridge.

ciated large negative gravity anomalies, extensive seismicity, and volcanism. Between 10.5°S and 14.5°S latitude, the trench axis is approximately 250 to 300 kilometers west of the crest of the western cordillera and attains a maximum depth of greater than 6,300 meters (Hayes, 1966; 1974).

The geology of the region is known only on a broad scale (Bellido, 1969). Many of the chronological and structural relationships between the eastern and western cordilleras have not been clearly defined. The eastern cordillera consists of highly folded and faulted Precambrian metamorphic and metamorphosed Paleozoic sedimentary rocks which have been intruded and overlain in places by Mesozoic and Cenozoic igneous rocks. Reverse and normal faults are well developed along and parallel to both flanks of the cordillera. In contrast, the front of the western cordillera is formed by the late Cretaceous Andean batholith. Cenozoic volcanic rocks predominate along the eastern slopes and form many of the higher peaks. Complex normal faulting is common throughout the batholith and the volcanic belt. East of the batholith are a succession of anticlines and synclines with associated reverse and thrust faults which are aligned with the northwest trending axes of the cordilleras. The coastal area consists principally of Quaternary sands and gravels and Cretaceous volcanic sedimentary rocks. The mapped faults are primarily normal and are both parallel and transverse to the coast line (Jenks, 1956; Bellido, 1969; Bellido and de Montreuil, 1972).

FORESHOCK, MAIN SHOCK, AND LARGER AFTERSHOCKS

An apparent foreshock (m_b = 5.0), which was felt in Lima and nearby communities, occurred on September 27, approximately 6 days prior to the main shock. It occurred within 20 kilometers of the main shock and is considered to be the initial event of the earthquake sequence.

The main shock of October 3 (M_S = 7.6) was located approximately 65 kilometers west-southwest of Lima, about 130 kilometers east of the Peru-Chile trench axis. It caused extensive damage in the Callao, La Molina, and Churrillos-Barranco districts of metropolitan Lima and to several coastal communities, e.g., San Luis, Cañete, and Chincha, located south-southeast of Lima. Partial or total collapse of adobe buildings and severe damage to some reinforced structures, particularly in La Molina, resulted from the intense shaking. Landslides and settling occurred close to the ocean shore along steep cliffs or embankments consisting of sands and gravels. The number of reported casualties include 78 killed and 2,414 injured (USGS, 1974b).

The sequence of aftershocks included numerous felt earthquakes and was essentially terminated, in a rather unusual manner, by a magnitude-7.2 (M_S) event on November 9 which caused additional damage to already weakened structures. Thirty-three hypocenters were determined from teleseismic data for the time period spanning approximately 12 weeks (Table 1). The aftershock magnitudes range from 4.0 (m_b), the apparent lower threshold for teleseismic locations near the coast of central Peru, to 7.2 (M_S; m_b = 6.0).

TABLE 1

LIST OF TELESEISMICALLY LOCATED EARTHQUAKES

NEAR LIMA, PERU, SEPTEMBER-DECEMBER, 1974

(12° to 14°S, 76° to 79°W)

Date (1974)	Origin Time (UTC)	Latitude (°S)	Longitude (°W)	Focal Depth (km)	Magnitude (m_b)	Magnitude (M_s)	Std. Dev. (sec)	No. of Stations	Remarks
Sept 27	16 09 03.7	12.427	77.576	18*	5.0	4.2	1.1	21	Felt (III), Lima
Oct 3	14 21 31.1	12.256	77.627	21*	6.3	7.6	1.0	165	Max. int. (VII)
	14 35 22.4	12.636	78.005	N	5.0		0.7	6	
	15 28 18.5	12.452	76.505	N	4.6		1.0	10	
	19 10 00.4	13.500	77.132	28	4.8		1.0	26	
	20 39 24.9	12.403	77.644	26*	4.8	4.8	0.9	26	
	20 49 32.6	12.459	78.116	N	4.6		0.8	6	
	21 56 57.2	13.430	77.029	22*	4.8	4.9	1.0	19	
	22 14 06.3	12.106	77.919	26	4.8		1.3	9	
Oct 4	02 34 30.2	13.462	77.121	26	4.3		1.0	17	
	12 47 39.7	12.098	77.527	54	4.1		1.4	9	Felt (II), Lima
	14 40 04.4	12.611	77.446	N	4.2		0.5	7	Felt (IV), Lima
	18 11 55.3	13.366	77.350	N	4.3		1.1	8	Felt (III), Lima
Oct 5	08 29 50.8	12.340	77.740	21*	4.7	4.2	1.1	15	Felt (IV), Lima
	17 57 59.8	13.760	76.639	23*	4.7		0.8	16	Felt (II), Lima
	20 08 44.2	12.811	77.757	N	4.4		1.0	7	Felt (III), Lima
Oct 6	03 50 25.4	12.461	77.739	19	4.3		0.7	11	Felt (II), Lima
Oct 7	04 57 51.4	12.246	77.939	26	5.0	4.7	1.0	26	Felt (V), Lima
	11 40 27.7	13.476	76.951	N	4.5		1.0	21	Felt (IV), Lima

TABLE 1--Continued

Date (1974)	Origin Time (UTC)	Latitude (°S)	Longitude (°W)	Focal Depth (km)	Magnitude (m_b)	Magnitude (M_S)	Std. Dev. (sec)	No. of Stations	Remarks
Oct 9	02 59 00.4	12.739	77.156	N	4.4		1.1	15	Felt (IV, Lima
	17 49 54.9	12.515	77.726	N	4.8		1.0	18	Felt (V), Lima
	21 54 32.2	12.879	76.874	N	4.9		1.1	18	Felt (V), Lima
Oct 10	19 52 59.0	12.444	77.606	19*	5.3	5.1	0.8	66	Felt (V), Lima
	20 57 47.5	12.994	77.543	24*	4.8	4.4	0.9	25	
Oct 12	01 08 01.2	13.408	77.402	N	4.2		1.2	7	
Oct 13	07 52 48.6	12.634	77.131	N	4.2		1.1	7	
	17 34 28.2	12.559	77.157	N	4.0		1.3	5	Felt (II), Lima
Oct 14	22 36 15.4	12.620	76.841	57	4.2		1.2	8	
Oct 24	02 25 39.2	12.531	77.304	60	4.5		0.9	7	Felt (II), Lima
Nov 2	00 57 37.1	12.528	77.869	N	4.9		1.3	20	
Nov 9	12 59 49.9	12.524	77.639	10*	6.0	7.2	1.0	131	Felt (V), Lima
Nov 14	19 17 35.2	12.848	77.078	N	5.4		0.9	55	Felt (III), Lima
Dec 24	00 54 00.5	12.864	77.963	19	4.7		1.2	13	

Data obtained from USGS (1974a, 1974b, and 1974c).
Reported intensities (MM) listed in parentheses under Remarks.
N: Normal depth (33 km).
*: Focal depths recomputed using depth phase (pP) data recorded at Albuquerque (ALQ) and Tucson (TUC).

REGIONAL AFTERSHOCK STUDY

Instrumentation and Field Procedure. Because many of the earthquakes occurred offshore, it was not possible to encircle completely the seismic source area with the monitoring network. Further constraints were also imposed by mountainous terrain and logistics. A maximum of ten stations was employed, three of which were permanent IGP observatories. Table 2 lists the seismograph locations and their respective recording time periods. The instrumentation used and seismometer site conditions are described in Table 3.

The first of five USGS systems was installed October 7 in the Miraflores section of Lima. Stations were later placed at Chilca, Huacho, Paracas, Canta, and Condor to augment the IGP instruments at Naña, Huancayo, Magdalene (Lima), Cañete, and Guadalupe. The resulting network length was approximately 375 kilometers, extending southeasterly from about 11°S to 14°S latitude (Figure 2) and was of sufficient size to bracket the aftershock zone in the north-south direction.

Precise time corrections were determined at the temporary sites with a WWV radio receiver and an oscilloscope. The overall network timing accuracy is within ±0.05 second except for Naña, Guadalupe, and Cañete. The accuracy at Naña is not definitely known; however errors are thought to be no greater than ±0.10 second (L. C. Ocola, personal communication). Early in the aftershock sequence, accurate time corrections were not made at Guadalupe or Canete. However, clock drift curves determined for these stations are, in general, quite linear. Use of extrapolation leads to an estimated ±0.20 second accuracy prior

TABLE 2

REGIONAL SEISMOGRAPH STATIONS USED

IN THE LOCATION OF AFTERSHOCKS

Station Name	Abbr.	Latitude (°S)	Longitude (°W)	Elevation (meters)	Magnification[1] ($x10^3$)	System Passband[2] (Hertz)	Period of Operation
Nana (IGP)	NNA	11.988	76.842	700	50	--	Permanent
Huancayo (IGP)	HUA	12.038	75.323	3,313	36	--	Permanent
Magdalena-Lima (IGP)	SP2	12.093	77.068	70	15	--	Permanent
Canete-Hotel (IGP)	CAH	13.073	76.388	31	∿500	1-30	Oct 4-Oct 5
Canete-Fundo (IGP)	CA1	13.067	76.397	32	∿500	1-30	Oct 5-Oct 24
Guadalupe (IGP	GU1	14.005	75.792	550	∿350	1-30	Oct 5-Nov 13
Miraflores-Lima (USGS)	MAR	12.118	77.038	68	22	1-30	Oct 7-Oct 12
Chilca (USGS)	CL1	12.518	76.793	90	43	5-30	Oct 8-Oct 25
Huacho (USGS)	HU1	11.092	77.572	75	43	1-10	Oct 8-Oct 19
Paracas-Hotel (USGS)	PA1	13.833	76.255	2	43	1-10	Oct 9
Paracas-Museo (USGS)	PA2	13,860	76.268	2	43	1-10	Oct 9-Oct 21
Canta (USGS)	CT1	11.462	76.623	2,837	22	1-30	Oct 11-Oct 17
Condor (USGS)	CON	13.548	75.533	1,550	344	5-30	Oct 14-Oct 22

[1]Magnifications for NNA, HUA, and SP2 are at 1 Hertz, all other systems are at 10 Hertz.
[2]The listed passbands indicate approximate 3db down points at the low and high ends of the recorder frequency response curve for the adjusted filter settings.

TABLE 3

INSTRUMENTATION AND SITE CONDITIONS
AT THE REGIONAL SEISMOGRAPH STATIONS

Station	Instruments		Seismometer Site
	Recorder	Seismometer	
NNA	[1]WWNSS	WWNSS	Concrete pier on bedrock
HUA	[2]WWNSS type	WWNSS type	Concrete pier in compacted alluvium, near bedrock
SP2	[3]Helicorder	J-M	Concrete floor on loosely consolidated conglomerates
CAH	[4]MEQ-800	S-7000	Concrete floor on unconsolidated sediments
CA1	[4]MEQ-800	S-7000	Concrete floor on compacted alluvium
CL1	[5]MEQ-800	L-4	Bedrock
HU1	[5]MEQ-800	L-4	Concrete floor on unconsolidated sediments
PA1	[5]MEQ-800	L-4	Concrete floor on sand
PA2	[5]MEQ-800	L-4	Sand
GU1	[6]MEQ-600	S-7000	Concrete pier on bedrock
MAR	[5]MEQ-800	L-4	Soil over unconsolidated conglomerates
CT1	[5]MEQ-800	L-4	Loosely consolidated conglomerate
CON	[5]MEQ-800	L-4	Bedrock

[1]Standard WWNSS system.
[2]1-component, short-period Z; 3-component, long-period.
[3]Heated stylus recorder (Teledyne-Geotech); 1-component, short-period Z (Geotech).
[4]Ink recorder (Sprengnether); 1-component, short-period Z (Sprengnether).
[5]Smoked paper recorder (Sprengnether); 1-component, short-period Z (Mark Products).
[6]Smoked paper recorder (Sprengnether); 1-component, short-period Z (Sprengnether)..

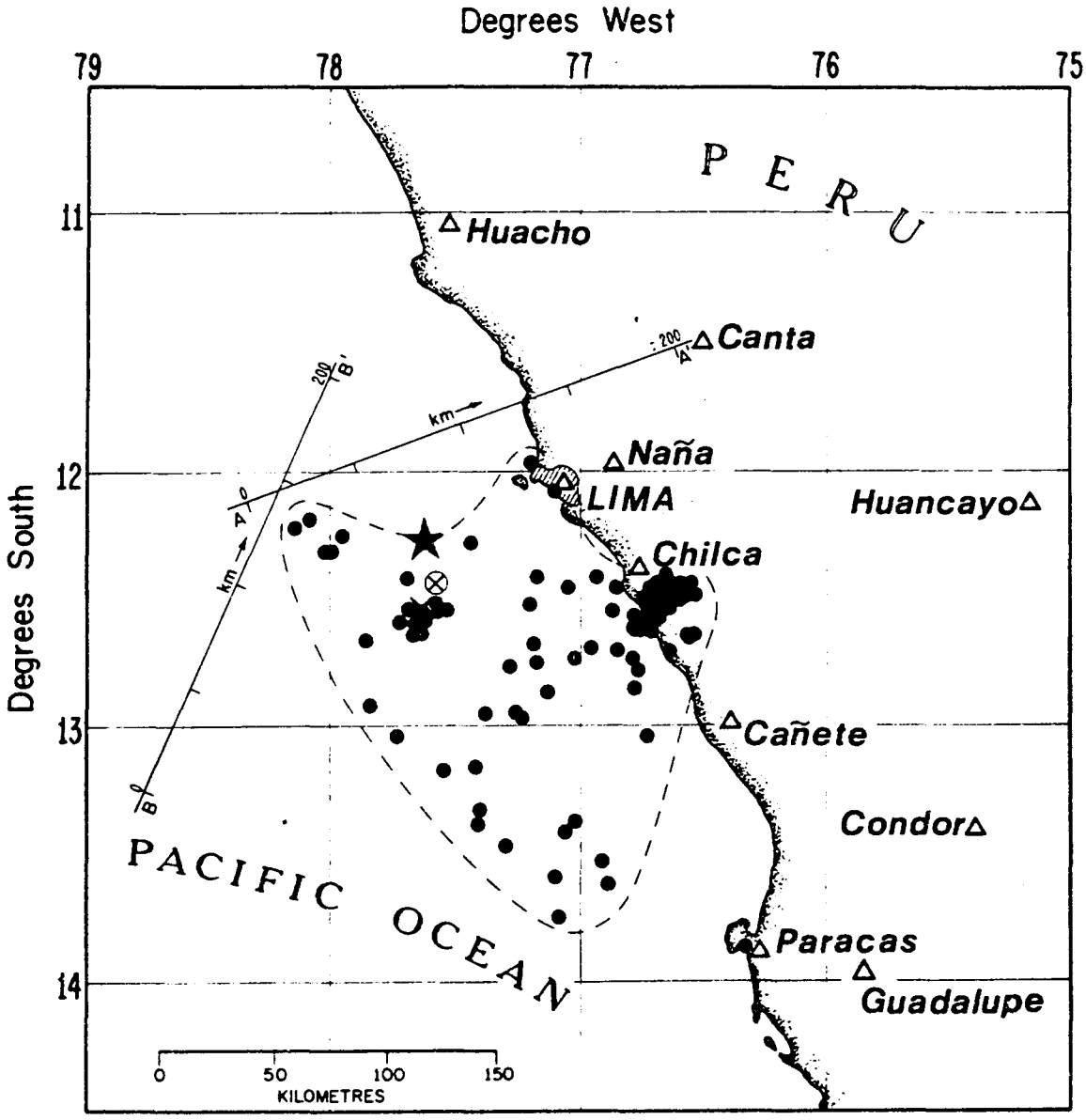

Figure 2. Spatial distribution of 113 aftershock epicenters and the regional seismograph network station locations. Symbols: star - main shock epicenter; large x - largest aftershock (November 9) epicenter; circle with x - foreshock epicenter; solid circle - after shock epicenter; open triangle - seismograph station location. Note that the foreshock, main shock, and November 9 event occur near the northern boundary of the aftershock zone. Sections A-A', B-B' used in Figure 5.

to October 9. Subsequent timing is at the previously stated network accuracy.

The recording speed for all seismographs was 60 millimeters/minute and the stylus deflection adjustments were set for maximum peak-to-peak amplitudes (~50 millimeters). Record quality at most stations was excellent (Figure 3).

Data Processing

Seismographs at distances greater than 150 km from an aftershock epicenter were at or near P_n range. Consequently, for the lower magnitude events, the onset of the first-motion was frequently small and sometimes partially obscured by the background noise. In order to improve the record-reading capability, enlargements (x2) were made of all the temporary station records. Phase arrival times were then measured with a low-power magnifier and corrected for any small variations in the length between minute marks. Arrival time accuracies for most P-phases are thought to be within ±0.1 second. For most aftershocks, S-phase arrivals were easily identified at two or more stations. The Naña data was particularly useful because of the short-period horizontal recordings. The estimated accuracy of selected S-times is approximately 1.25 seconds.

A five-layer P-wave velocity model (Table 4) and a P-to-S velocity ratio of 1.76 (Poisson's ratio ≈0.26) were assumed for the aftershock zone to compute the hypocentral locations. The P-wave model is based on Woollard's (1975) marine air gun observations and land explosive measurements which extended in an east-west profile across the Nazca

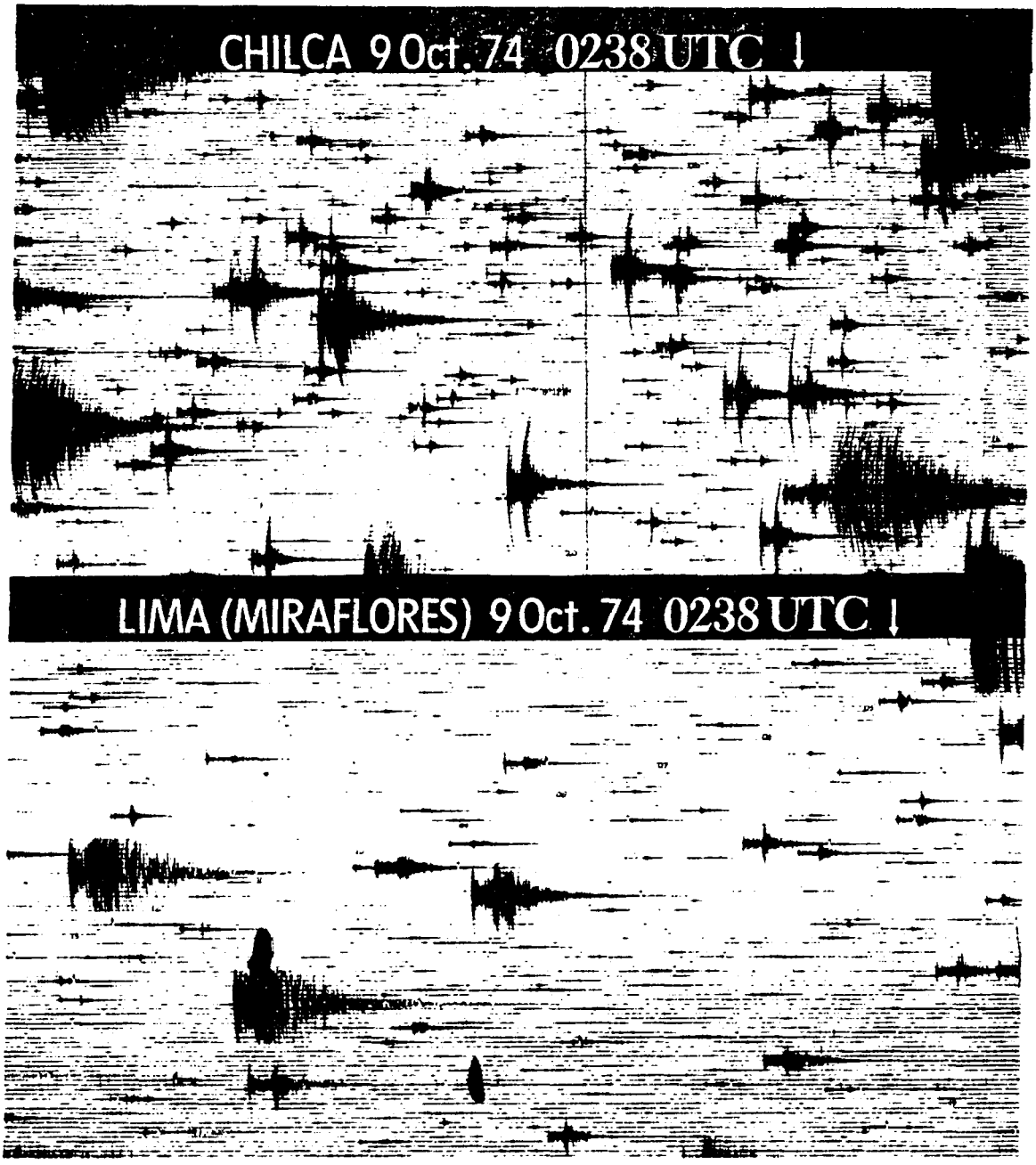

Figure 3. Seismograms from portable stations at Chilca and Lima (Miraflores) showing contrast in seismicity. On original records the trace separation is 1 mm and the distance between minute marks is 60 mm. Time period and seismograph magnifications are approximately equivalent.

TABLE 4

VELOCITY MODEL FOR THE PERUVIAN COAST
BETWEEN 10° AND 11°S LATITUDE

(Woolard, 1975)

Layer Thickness (km)	P-Wave Velocity (km/sec)
1.0	4.5
2.5	5.8
18.5	6.3
8.0	7.5
---	8.0

plate onto the continent at about 10.5°S latitude. Other P-velocity structures for the region of interest have been derived by Hussong (1972), Ocola and Meyer (1973), Johnson et al. (1973), and Hussong et al. (1976); however, the Woollard model is preferred because use of the other models consistently gave larger travel-time residuals at most stations. The P-to-S velocity ratio was determined by L. C. Ocola (personal communication) from refraction data obtained from profiles across central and southern Peru.

Of the several thousand aftershocks detected by the seismograph network, 113 hypocentral locations (Table 5) were determined with the HYPO 71 computer program (Lee and Lahr, 1975). A measure of the hypocentral accuracies is indicated by the standard errors, the average of which are about ±4.1 kilometers in the horizontal plane and ±3.0 kilometers in the vertical plane. These values, however, may not represent the actual error limits because the statistical interpretation involves the assumption that the errors are random and not affected by station distribution or anomolous seismic velocities. In this study, the hypocentral solution quality is somewhat degraded by the large azimuthal gap in the aftershock network and the complex velocity structure common to zones of plate subduction.

James et al. (1969) have discussed some of the problems in obtaining satisfactory hypocentral solutions for local earthquakes in Peru when using small seismograph networks (<10 stations); however, their investigation was based on instabilities inherent in the most refined hypocenter location programs of that time (e.g., Bolt, 1960; Cisternas, 1964; Engdahl and Gunst, 1966). HYPO71 was designed specifically for

TABLE 5

AFTERSHOCKS OF THE PERUVIAN EARTHQUAKE OF OCTOBER 3, 1976,
LOCATED BY TEMPORARY SEISMOGRAPH NETWORK

Date (Oct. 1974)	Origin Time (UTC)	Lat. S (deg)	Long. W (deg)	Depth (km)	No.[1] Sta.	DMIN[2] (km)	RMS[3] (sec)	Standard Errors[4] DLAT (km)	DLON (km)	DZ (km)	M_L[5]
7	0457 50.69	12.172	78.093	22.5*	7	121	0.13	2.8	1.7	4.0	5.0
7	1140 28.43	13.523	76.914	16.8	7	75	0.25	1.9	3.4	3.6	4.6
7	1325 34.45	12.460	76.556	48.0	7	61	0.11	1.9	3.1	3.6	3.5
7	1541 33.86	12.533	76.689	25.7	7	60	0.14	1.7	2.7	3.7	---
7	1542 56.33	12.574	76.763	46.1	8	59	0.21	3.8	6.0	4.0	4.0
7	2204 11.97	12.649	77.864	24.0*	7	106	0.09	1.1	1.8	1.7	4.7
8	0525 42.18	12.460	76.663	51.6	7	56	0.09	1.7	2.8	2.3	4.0
8	1144 14.28	12.452	76.704	58.7	7	52	0.19	3.6	5.9	3.8	3.9
8	1805 33.14	12.463	76.704	59.5	8	53	0.13	2.2	3.5	2.1	4.3
9	0212 16.11	12.518	76.719	55.7	8	8	0.10	1.8	3.0	1.1	4.1
9	0221 20.41	12.516	76.684	60.0	9	12	0.16	2.8	4.4	2.4	3.9
9	0259 04.37	12.573	76.758	49.9	10	7	0.10	1.4	2.4	1.2	4.4
9	0359 26.20	12.598	76.781	47.2	9	9	0.10	1.9	3.0	0.9	2.5

TABLE 5--Continued

Date (Oct. 1974)	Origin Time (UTC)	Lat. S (deg)	Long. W (deg)	Depth (km)	No.[1] Sta.	DMIN[2] (km)	RMS[3] (sec)	Standard Errors[4] DLAT (km)	DLON (km)	DZ (km)	M_L[5]
9	0412 59.05	12.518	77.204	27.2	9	48	0.15	1.6	1.8	3.3	3.0
9	0439 36.14	12.587	76.715	47.3	10	11	0.27	3.8	6.1	2.0	2.6
9	0551 15.68	12.518	76.672	59.6	10	13	0.23	3.2	5.3	2.8	3.6
9	0942 13.30	12.619	76.783	44.2	11	11	0.22	2.9	4.6	2.7	3.0
9	0956 55.17	12.464	76.674	43.7	10	14	0.29	2.3	4.6	3.5	3.1
9	1002 51.32	12.596	76.773	38.7	10	9	0.25	3.1	5.1	3.0	2.8
9	1038 10.91	12.520	76.705	57.5	11	10	0.22	2.8	4.5	2.3	3.8
9	1045 27.50	12.639	77.675	21.7	9	89	0.26	1.9	2.2	4.1	3.4
9	1245 08.27	12.242	77.956	25.0	8	98	0.18	2.0	1.7	2.8	2.9
9	1339 16.74	12.605	76.741	50.1	11	11	0.16	2.2	3.5	1.2	2.7
9	1416 38.28	12.566	76.787	50.4	11	5	0.21	1.5	3.1	1.3	---
9	1459 54.41	12.631	77.668	25.2	8	88	0.13	1.2	1.8	3.6	3.1
9	1522 30.07	12.514	76.716	56.7	10	8	0.20	2.7	4.7	2.7	3.8
9	1727 32.86	12.462	76.659	40.1	10	16	0.20	2.3	3.9	3.3	3.0

TABLE 5--Continued

Date (Oct. 1974)	Origin Time (UTC)	Lat. S (deg)	Long. W (deg)	Depth (km)	No.[1] Sta.	DMIN[2] (km)	RMS[3] (sec)	Standard Errors[4] DLAT (km)	DLON (km)	DZ (km)	M_L[5]
9	1749 36.82	12.537	77.537	14.6	10	71	0.17	1.1	1.3	1.4	---
9	1749 55.14	12.578	77.625	25.8	9	81	0.25	2.1	2.8	7.3	4.9
9	1814 24.46	12.513	77.580	15.6	8	72	0.11	1.2	1.8	0.9	3.6
9	1922 57.99	12.490	76.748	51.2	8	6	0.17	3.0	5.0	1.9	3.0
9	2007 41.65	12.409	76.938	49.7	9	20	0.17	1.3	2.2	1.8	2.6
9	2032 55.59	12.614	76.761	59.5	7	11	0.29	5.3	10.8	2.8	3.2
9	2119 20.58	12.444	76.682	50.4	8	15	0.31	4.3	8.2	3.8	3.8
9	2154 11.20	12.269	77.446	31.7	7	45	0.15	1.2	1.4	6.0	---
10	0009 08.64	12.746	77.181	28.2	8	71	0.28	2.6	3.5	5.4	3.5
10	0510 47.93	12.475	76.575	55.0	11	24	0.21	3.0	4.9	3.2	3.6
10	0516 43.38	12.434	76.553	50.0	11	28	0.25	3.2	5.3	4.4	3.7
10	0637 02.72	12.482	76.709	53.7	10	10	0.26	3.4	6.1	2.3	3.7
10	0845 23.88	12.637	76.545	40.0	11	30	0.30	3.7	6.0	5.5	3.7
10	1050 00.52	12.501	76.606	53.4	10	20	0.21	3.1	5.1	2.9	3.0
10	1051 11.71	12.750	77.286	22.3	11	60	0.16	0.7	1.9	4.5	3.9

TABLE 5--Continued

Date (Oct. 1974)	Origin Time (UTC)	Lat. S (deg)	Long. W (deg)	Depth (km)	No.[1] Sta.	DMIN[2] (km)	RMS[3] (sec)	Standard Errors[4] DLAT (km)	DLON (km)	DZ (km)	M_L[5]
10	1536 06.61	12.456	76.681	47.5	11	14	0.19	2.4	4.0	2.7	3.6
10	1953 00.58	12.537	77.634	22.7	10	79	0.13	0.8	1.0	2.4	5.2
10	2051 53.93	12.308	78.029	09.9	9	107	0.17	1.0	1.9	2.1	4.2
10	2057 45.79	13.166	77.558	10.6	10	109	0.22	3.3	1.7	5.3	4.8
10	2231 05.83	13.584	77.110	25.0*	10	96	0.29	1.6	2.8	5.9	4.0
10	0023 15.79	12.538	76.645	57.1	8	16	0.12	1.3	2.2	1.7	3.5
11	0329 30.05	12.310	78.009	22.6	11	105	0.19	1.1	1.7	3.8	4.1
11	0849 54.20	12.865	77.132	20.5	10	53	0.21	1.1	2.2	1.7	4.0
11	1409 26.43	13.324	77.405	13.0	11	111	0.29	2.4	2.7	5.4	3.9
11	1658 51.45	12.415	77.693	14.8	11	77	0.24	1.3	1.8	1.4	4.5
11	1747 55.59	12.964	77.233	13.1	12	69	0.29	1.5	2.2	2.6	3.9
11	1948 20.78	12.408	77.175	39.9	12	35	0.26	1.1	2.3	2.4	3.5
11	2102 35.99	12.594	77.669	14.8	11	86	0.15	0.7	0.8	0.8	4.0
11	2243 12.38	12.621	76.712	45.2	11	14	0.19	1.7	2.8	2.2	3.4
11	2336 18.20	12.534	76.686	58.4	11	12	0.18	0.9	2.0	1.6	3.3

TABLE 5--Continued

Date (Oct. 1974)	Origin Time (UTC)	Lat. S (deg)	Long. W (deg)	Depth (km)	No.[1] Sta.	DMIN[2] (km)	RMS[3] (sec)	Standard Errors[4] DLAT (km)	DLON (km)	DZ (km)	M_L[5]
12	0108 00.93	13.377	77.416	11.0	10	116	0.25	2.5	4.9	4.2	4.2
12	0137 37.08	12.517	76.684	47.2	11	12	0.26	1.7	3.5	3.0	3.5
12	1054 04.03	12.913	77.849	5.3	11	123	0.22	1.3	1.5	1.8	4.0
12	2005 09.73	13.611	76.891	14.4	10	73	0.23	1.8	2.5	2.2	3.7
12	2358 24.39	13.151	77.423	12.1	10	98	0.32	1.7	3.34	2.44	3.6
13	0203 41.55	13.738	77.091	1.8	9	90	0.29	2.6	2.4	2.7	3.6
13	0444 44.23	12.402	76.656	48.1	9	50	0.17	0.9	2.1	2.7	3.2
13	0752 53.97	12.447	76.554	56.6	10	60	0.27	2.0	3.5	3.8	4.3
13	0753 40.03	12.444	76.602	29.2	7	64	0.23	1.8	3.84	4.0	4.1
13	0801 37.26	12.428	76.536	44.4	9	59	0.17	1.3	2.2	3.7	3.9
13	0816 40.43	12.436	76.643	62.6	9	54	0.23	1.2	2.6	3.9	3.6
13	0840 47.75	11.965	77.202	65.5	8	20	0.10	0.8	1.4	1.6	3.9
13	0931 23.92	12.444	76.578	64.6	9	58	0.28	2.2	4.1	4.7	3.8
13	1734 32.23	12.473	76.614	43.0	8	59	0.24	3.2	5.3	5.4	4.2
13	2302 11.92	12.531	76.695	53.7	9	62	0.28	2.2	5.0	3.4	3.6

TABLE 5--Continued

Date (Oct. 1974)	Origin Time (UTC)	Lat. S (deg)	Long. W (deg)	Depth (km)	No.[1] Sta.	DMIN[2] (km)	RMS[3] (sec)	Standard Errors[4] DLAT (km)	DLON (km)	DZ (km)	M_L[5]
14	1336 41.00	12.731	76.794	20.0	9	57	0.35	2.1	3.4	3.3	4.1
14	1819 31.92	12.513	76.684	52.14	9	12	0.25	1.54	4.2	3.1	3.6
14	2236 15.18	12.692	76.968	49.7	9	27	0.28	3.44	6.24	4.3	4.1
15	0206 47.22	12.674	77.192	20.8	10	47	0.32	1.6	2.3	1.9	3.8
15	0333 19.40	12.440	76.690	53.5	9	14	0.28	2.0	4.3	3.3	3.5
15	1145 49.34	12.510	76.654	59.7	10	15	0.25	2.04	3.9	2.3	3.5
15	1248 25.49	12.606	76.790	51.7	9	10	0.25	2.6	4.7	1.9	3.6
15	1829 58.83	12.568	76.687	52.1	8	13	0.19	3.5	5.6	3.1	4.0
16	0305 00.17	13.410	77.067	25.0	9	82	0.18	1.0	1.7	3.7	3.8
16	0504 05.06	13.031	76.732	49.0	10	37	0.24	2.8	5.3	3.8	3.7
16	1025 22.41	12.697	76.857	37.3	11	21	0.26	2.1	3.8	2.6	4.0
16	1505 39.10	12.520	76.725	63.0	10	7	0.21	1.6	3.8	1.6	3.4
16	1640 00.13	12.614	76.764	38.8	11	11	0.28	1.8	3.5	3.0	3.4
17	0653 34.93	12.705	76.639	49.3	10	27	0.24	2.3	3.9	2.3	3.0
17	0825 42.39	12.481	76.730	46.8	10	8	0.24	1.64	3.3	2.6	3.1

TABLE 5--Continued

Date (Oct. 1974)	Origin Time (UTC)	Lat. S (deg)	Long. W (deg)	Depth (km)	No.[1] Sta.	DMIN[2] (km)	RMS[3] (sec)	Standard Errors[4] DLAT (km)	DLON (km)	DZ (km)	M_L[5]
17	0833 39.42	12.540	76.875	58.7	10	9	0.26	2.4	3.7	3.0	3.3
17	0931 21.45	12.642	76.548	42.5	10	30	0.27	2.4	4.3	3.5	3.1
17	2038 48.55	12.544	77.574	17.0	10	74	0.33	2.4	2.6	3.2	3.7
18	0501 11.25	12.635	77.637	13.0	8	86	0.27	1.3	1.9	1.5	3.6
18	1326 42.03	12.493	76.574	58.1	8	24	0.10	1.8	2.8	2.0	3.1
19	0616 28.33	12.456	76.721	41.7	9	10	0.18	1.8	3.1	2.5	3.3
19	0623 05.66	12.849	76.788	43.2	8	37	0.28	3.7	6.3	6.1	3.3
19	0828 22.68	12.942	77.254	16.0	10	69	0.17	0.8	1.4	1.3	3.6
19	1522 17.48	12.591	76.750	44.9	10	9	0.25	1.7	2.7	3.7	3.0
19	2036 13.29	12.211	78.151	20.0*	10	119	0.15	1.7	3.4	4.6	4.2
19	2320 19.07	12.733	77.026	31.5	8	35	0.11	0.7	1.9	2.8	3.4
20	0420 22.17	12.772	76.765	52.14	8	28	0.19	4.0	6.0	2.0	3.6
20	1414 12.32	12.563	76.729	51.6	10	9	0.26	2.8	3.9	2.1	3.4
20	2229 15.35	12.580	77.729	22.8	9	90	0.17	1.2	1.9	4.6	4.1
21	0301 18.08	13.373	77.024	8.7	9	76	0.09	0.6	0.9	0.6	3.6

TABLE 5--Continued

Date (Oct. 1974)	Origin Time (UTC)	Lat. S (deg)	Long. W (deg)	Depth (km)	No.[1] Sta.	DMIN[2] (km)	RMS[3] (sec)	Standard Errors[4] DLAT (km)	DLON (km)	DZ (km)	M_L[5]
21	0444 28.22	12.642	76.564	45.5	10	28	0.32	3.1	4.3	3.4	3.5
21	1318 48.03	12.531	77.695	25.0	9	84	0.23	1.7	2.6	5.4	4.1
22	0834 44.21	13.863	76.327	11.7	8	60	0.28	2.0	2.0	3.7	3.6
23	0347 56.07	13.036	77.735	19.0*	8	117	0.28	2.4	6.6	7.5	3.4
23	1053 09.40	12.561	76.713	49.94	8	10	0.21	4.0	6.3	2.4	3.0
23	1539 23.91	12.605	76.754	43.2	7	11	0.14	3.0	4.7	2.6	3.4
23	1644 42.85	12.079	77.104	47.0	7	4	0.06	0.9	1.7	0.9	4.0
23	1931 15.70	13.460	77.310	7.4	7	108	0.16	1.3	1.6	2.1	4.1
23	2231 18.38	12.451	76.858	42.5	8	10	0.10	1.4	2.4	0.8	3.4
24	0225 34.17	12.947	77.388	15.0*	7	80	0.26	1.8	2.9	2.3	4.4
24	0619 36.44	12.448	77.048	41.2	8	29	0.24	3.6	6.0	3.5	3.2

[1]No. Sta. - Refers to the number of phases used to obtain hypocentral solutions.
[2]DMIN - Distance to the closest seismograph station.
[3]RMS - Root mean square errors of travel time residuals.
[4]Standard errors - Refers to the statistical indices of precision, as defined by Draper and Smith (1966), which are related to the values and distribution of the unknown errors in the hypocentral solution where DLAT = error in latitude, DLON = error in longitude, and DZ = error in depth (Lee and Lahr, 1975).
[5]M_L - Local magnitude of aftershock.

*Denotes fixed depth.

determining local earthquake hypocenters using a multi-layer flat-earth velocity model. A step-wise multiple regression technique is employed to solve the normal equations (Geiger, 1910) which stabilizes the matrix formed from the normal equations and prevents it from becoming ill-conditioned (Lee and Lahr, 1975). The inclusion of accurate S-phase data greatly improves the solution quality, particularly for hypocenters located outside the seismograph network. To minimize the possibility of large errors in locations, the number of data used for any one solution include not less than five P- and two S-readings.

Location of Aftershocks.

Aftershock epicenters are confined within an irregularly shaped region (Figure 2), the southwestern side of which trends southeast, roughly parallel to the coast, between about 12.2°S and 13.8°S latitude. The zone, which is approximately 210 kilometers long by 150 kilometers wide, extends onto the coast in the vicinity of Chilca and also near Lima. The aftershocks exhibit a fairly uniform pattern throughout the area with the exception of the dense cluster south of Chilca and the group of ten epicenters south of the main shock epicenter. The cluster near Chilca consists of 59 events and reflects a much higher degree of seismic activity than observed at other network stations (Figure 3). Control from nearby seismographs to the northwest (Naña and Lima) and to the southeast (Cañete), as well as Chilca, lend validity to the continental or near continental locations of these epicenters.

In order to investigate a more uniform sample in terms of the distribution of aftershock energy release, only the largest and, therefore, best located aftershocks ($M_L > 4.0$) were selected (Figure 4). This epicentral plot indicates a southwest trend, perpendicular to the coast, extending outward from the Chilca cluster to the southwestern margin of the aftershock zone as well as a pronounced southeasterly trend of the oceanward events. In addition, the concentrations of aftershocks south of the main shock epicenter and, particularly, those south of Chilca are still much in evidence. This suggests that the large number of events located near Chilca is not merely a function of station distribution but is a unique feature of the aftershock zone.

The vertical distribution of aftershocks is presented in Figure 5 by means of two cross sections, each of which is perpendicular to a nodal plane of the main shock focal mechanism (Figure 7). Depths range from near surface for the more oceanward events to about 66 km for those aftershocks in the vicinity of Chilca. The dip inferred from the hypocentral locations is consistent with shallow underthrusting indicated by the main shock focal mechanism (Spence, et al., 1976).

A comparison of all epicenters determined from both teleseismic and regional network data (Table 6) is shown in Figure 6. Of these eleven aftershocks, the magnitude-5.3 (m_b) event on October 10 at 1953 (UTC) is the largest and may therefore be considered to have the best teleseismic location. The regionally determined epicenter is located approximately 10 kilometers south-southeast of the teleseismically determined epicenter. The general trend of the difference in locations for the oceanward events ranges southwest to southeast whereas the trend of four of

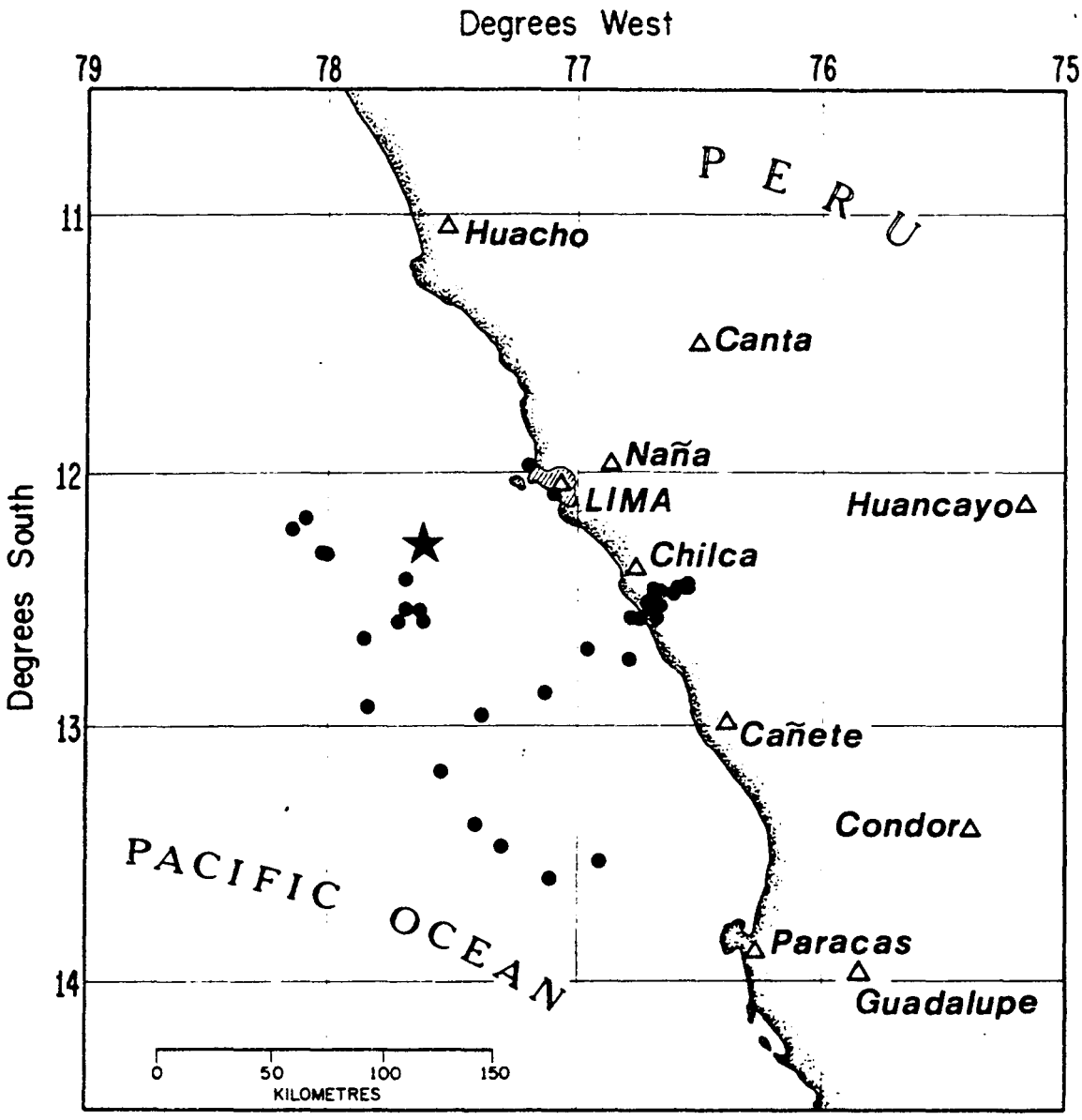

Figure 4. Epicentral locations of the larger aftershocks (M_L > 4.0). Symbols the same as for Figure 2.

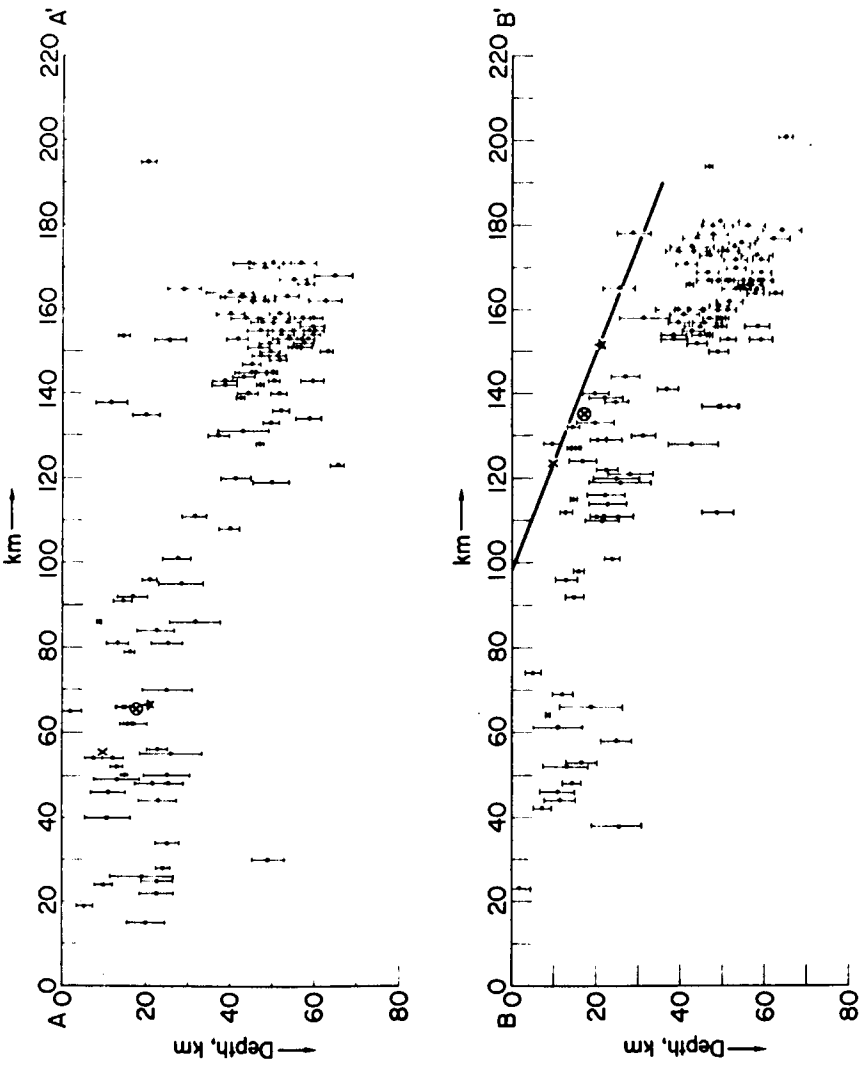

Figure 5. Vertical cross sections showing depth distribution of the aftershock hypocenters and associated error-bars. Each hypocenter is projected into planes perpendicular to the main shock focal mechanism nodal planes. Section A-A' is normal to the N20°W nodal plane; B-B' is normal to the preferred or N66°W nodal plane. Symbols are the same as in Figure 2; sections A-A', B-B' also shown in Figure 2. Heavy line in section B-B' represents projection of preferred nodal plane of main shock focal mechanism; strike is N20°W, dip is 21°.

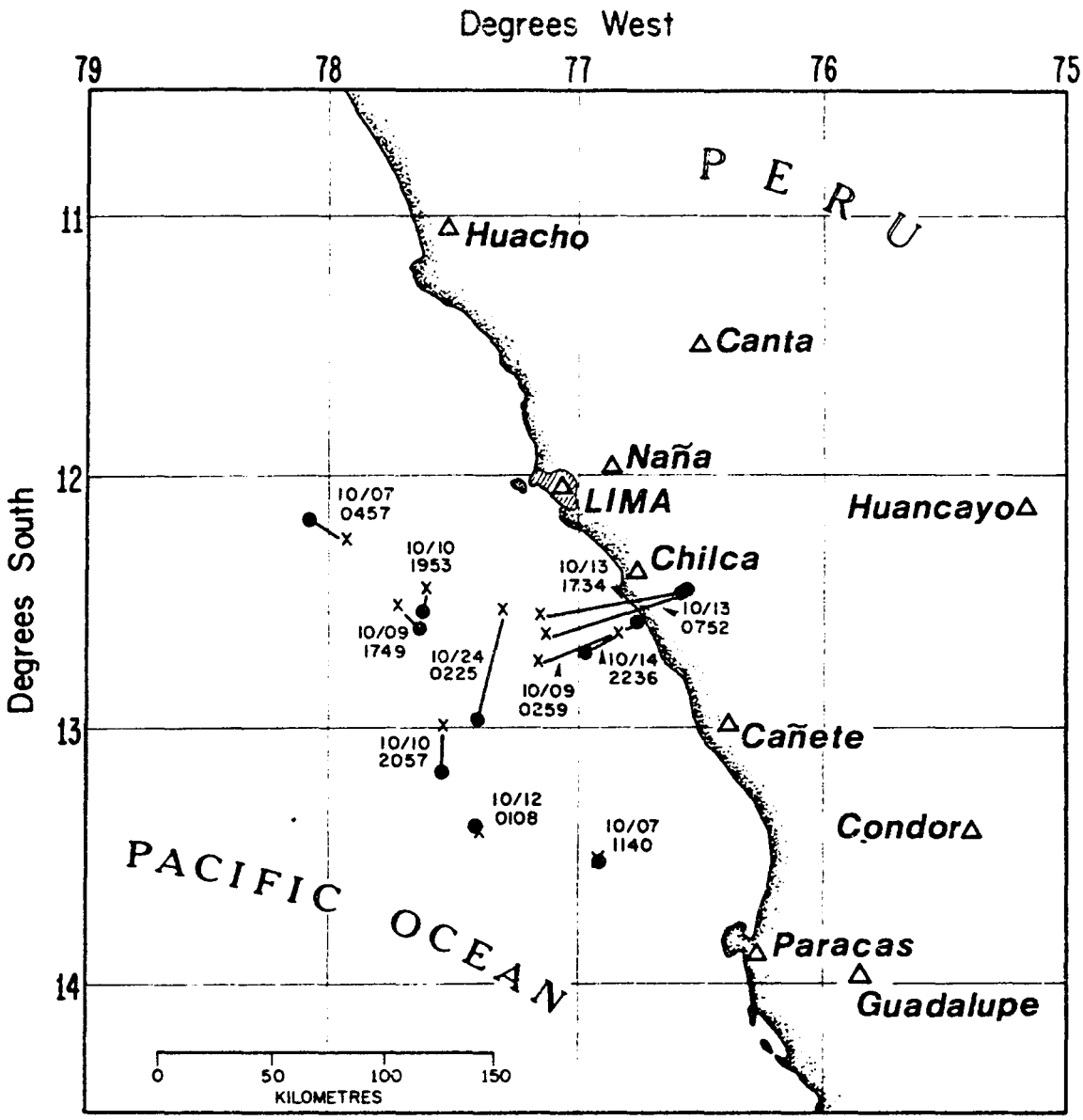

Figure 6. Teleseismic and regional epicenter comparisons. Lines connect equivalent epicenters where a solid circle represents a regional location and an x denotes a teleseismic location. Date and origin time (UTC) shown by each epicenter pair.

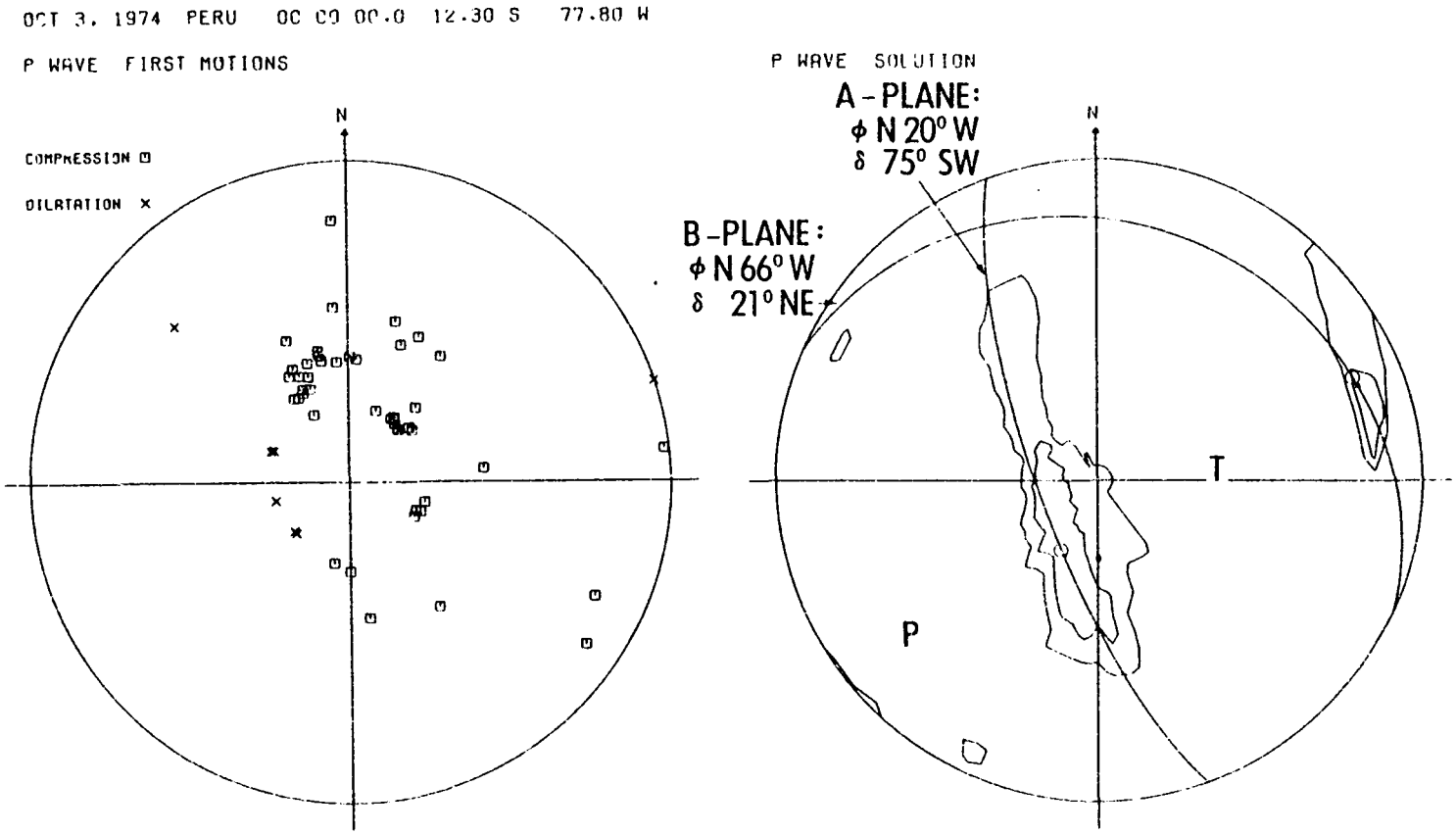

Figure 7. Long-period P-waves first motion data and corresponding lower hemisphere equal-area projection of the focal mechanism solution for the October 3, 1974, main shock. Compressional axis is denoted by a P, the tensional axis by a T, and the poles of each plane by a small circle. The contours indicate fiducial levels associated with the number of consistent observations (Dillinger, et al., 1972), the inner contours having the highest number of consistent observations. For this solution there are three inconsistent readings associated with the innermost contours.

TABLE 6

COMPARISON BETWEEN TELESEISMICALLY AND
REGIONALLY LOCATED AFTERSHOCKS

Date (1974)	Origin Time UTC	No. of Sta.[1] Tel.	Reg.	Magnitude M_b	M_L	Epi. Diff.[2] (km)	Depth of Focus (km) Tel.	Reg.
Oct. 7	0457	26	7	5.0	5.0	17	26	23
	1140	21	7	4.5	4.6	1	N	17
Oct. 9	0259	15	9	4.4	4.4	47	N	50
	1749	18	9	4.8	4.9	12	N	26
Oct. 10	1953	66	10	5.3	5.2	10	19	23
	2057	25	10	4.8	4.8	19	24	11
Oct. 12	0108	7	10	4.2	4.2	4	N	11
Oct. 13	0752	7	10	4.2	4.2	62	N	57
	1734	5	8	4.0	4.2	65	N	43
Oct. 14	2236	8	9	4.2	4.1	16	57	50
Oct. 24	0225	7	7	4.5	4.4	50	60	41

[1]No. of Sta. - Refers to the number of stations used for teleseismic (Tel.) location or number of phases used for regional (Reg.) location.
[2]Epi. Diff. - Indicates distance between teleseismic and regional locations for the same aftershock.
N - Denotes normal depth of focus (33 kilometers).

the more coastal aftershocks is east-northeast. Expectably, the greatest location differences are associated with the deeper (>40 kilometers) aftershocks.

Within the scope of this study, it cannot be stated explicitly whether the regionally located epicenters are more or less accurate than those determined by teleseismic data. Algermissen, et al. (1974) show that the epicenter reported by NOAA (1973) for the Managua, Nicaragua, earthquake of December 23, 1972 (M_S = 6.2) was mislocated approximately 25 kilometers to the northeast. They argue that the errors in location are due primarily to the bias introduced by the teleseismic station distribution and the anomously high velocities related to the Benioff zone. Similar conditions also exist for western South America although, in the area of study, location errors are somewhat reduced by control from the Peruvian seismograph stations. Travel time errors for the regional seismograph network are considered to be significantly less than for seismographs at teleseismic distances because of shorter hypocenter-to-station seismic ray paths. Therefore, in most cases, the regionally determined aftershock locations are thought to be more precise than the locations determined from teleseismic records.

FOCAL MECHANISM SOLUTIONS

A focal mechanism for the main shock (Figure 7) was determined by Spence et al. (1976) from 56 long-period P-wave first-motion observations using the method of Dillinger et al. (1972). Although this solution is not unique, i.e., the elliptical fiducial areas indicate a well controlled dip but a poorly controlled strike, the preferred nodal plane (B-plane) is representative of shallow underthrusting and is therefore in accordance with the subduction of the Nazca plate beneath continental Peru. This solution is in general agreement with the results of Stauder (1975) and Wagner (1972) for five earthquakes of normal focal depth near the central Peruvian coastline. There is also a close correspondence with the focal mechanisms of Isacks and Molnar (1971) for six intermediate depth earthquakes between southern Ecuador and central Peru. Thus, a similarity in stress distribution at both the shallow and intermediate depths of the descending lithosphere is indicated.

The thirteen aftershocks ($M_L \geq 4$, Figure 4) located in a group south and in a line southwest of Chilca were used to construct the composite focal mechanism solution (CFMS) shown in Figure 8. The strike and dip of the preferred nodal plane (A-plane) are well constrained and comparable with the preferred nodal plane of the main shock. A dip of 30° is somewhat greater than would normally be expected, however, this parameter is quite sensitive to the velocity model of HYPO71 and may therefore be reflecting some of the inconsistency between the actual structure and the assumed model. The

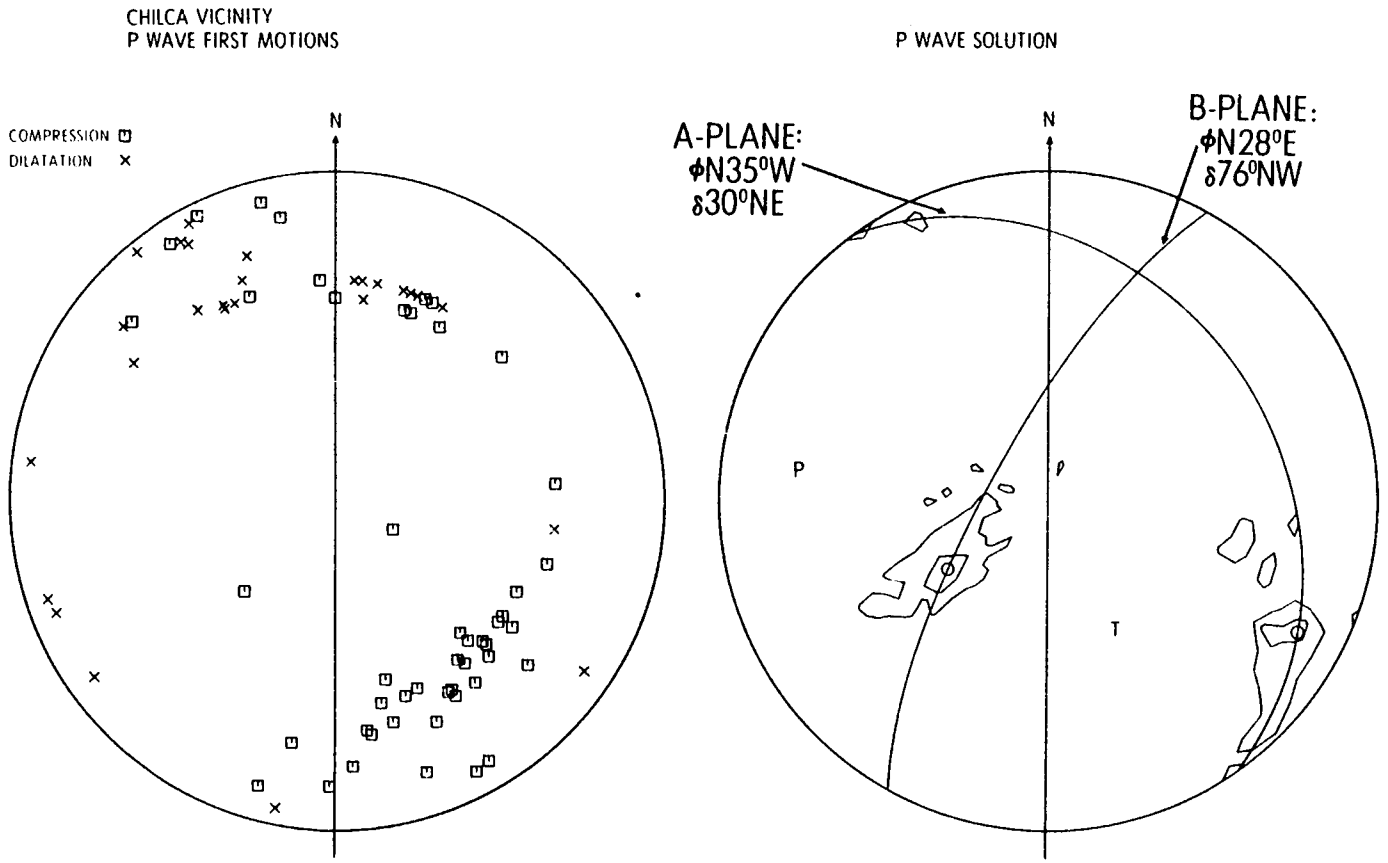

Figure 8. Composite focal mechanism solution (lower hemisphere) of 13 aftershocks in the vicinity of Chilca. Contours and symbols are described in Figure 7. Of the 76 P-wave first-motion data, there are 66 consistent observations. The innermost contours represent an interval between 66 and 63 consistent readings.

strike is nearly parallel to that of the coastline and in excellent agreement with the previously reported focal mechanism solutions for coastal Peru.

STATISTICAL PROPERTIES

Magnitudes

Local magnitude estimates, M_L, (Table 5) were computed using the coda-length technique applied by Lee et al. (1972) to earthquakes in California. Conventional magnitudes (Richter, 1958) could not be determined, for the most part, because the maximum recorded P- and S-phase amplitudes were either instrumentally clipped or not discernible.

For the period October 7-24, there are 32 aftershocks of magnitude $M_L \geq 4.0$ but only the eleven listed in Table 6 have been located teleseismically. However, 17 of these 32 are at the lower magnitude threshold (4.0-4.1) for teleseismic location within the area of study. Since the magnitudes of the eleven teleseismically located events compare favorably with corresponding local magnitudes (Table 5), it is assumed that the listed M_L values are, within a reasonable degree of accuracy (±0.3), representative of the actual aftershock magnitudes. A careful examination of the regional data indicate that the four aftershocks of magnitude $M_L \geq 4.2$ which were not located teleseismically are not anomalous. This suggests that adequate readings were not provided to the USGS National Earthquake Information Service (NEIS, Golden, Colo.) for satisfactory teleseismic locations.

Magnitude-Frequency Relationships

An empirical relationship between earthquake magnitudes and their frequency of occurrence is expressed by Gutenberg and Richter (1954) as

$$\log N(M) = K - bM$$

where N(M) equals either the incremental number (N_i) or cumulative number (N_c) of earthquakes of magnitude M, and K and b are constants. The value of $N_i(M)$ is defined explicitly by Page (1968) and represents the number of earthquakes within a selected magnitude interval range. The significance and statistical nature of the slope or b value of the resulting curve have been discussed in detail by numerous investigators (e.g., Isacks and Oliver, 1964; Utsu, 1967; Page, 1968; Karnik, 1971).

It is often difficult to apply a valid interpretation to many of the reported b values because the data sets are statistically incomplete and/or the method of computation is not clearly described. Also, some authors ignore the difference in the relation between $N_c(M)$ and $N_i(M)$, i.e., that $b_c \geq b_i$ (Karnik, 1971).

For the purposes of this study, $N_i(M)$ is used to determine values of b by the following three methods: (1) least squares which assumes a continuous random quantity obeying the Gaussian distribution; (2) weighted least squares which introduces weights for individual points (Karnik and Prochazkova, 1971), otherwise the same as least squares; and (3) the Page (1968) maximum likelihood method. The values of b listed in Table 7 illustrate the results from these methods of computation and show that, for these data, they yield comparable b values. Figure 9 shows the distribution of magnitudes used for the calculations of b and also the cumulative distributions over the entire range of observable magnitudes. The magnitude data for the shallow seismic belt of coastal Peru were provided by the National Oceanic and Atmospheric

TABLE 7

VALUES OF b DETERMINED FROM 1974 REGIONAL AFTERSHOCK DATA AND EARTHQUAKES ORIGINATING WITHIN THE PERUVIAN SHALLOW SEISMIC BELT (1963-1975)

Region	No. of Earthquakes	Magnitude Range	Method[1]	b
A. Aftershock Zone	74	3.6-5.2(M_L)	(1)	0.86±0.04
			(2)	0.86±0.05
			(3)	0.89±0.24
B. Shallow Seismic Belt	316	4.6-6.6(m_b)	(1)	0.88±0.02
			(2)	0.86±0.02
			(3)	0.94±0.18

[1]Method (1): Least squares and associated standard error.
(2): Weighted least squares and associated standard error
(3): Page (1968) maximum likelihood and approximate 95 percent confidence limits.

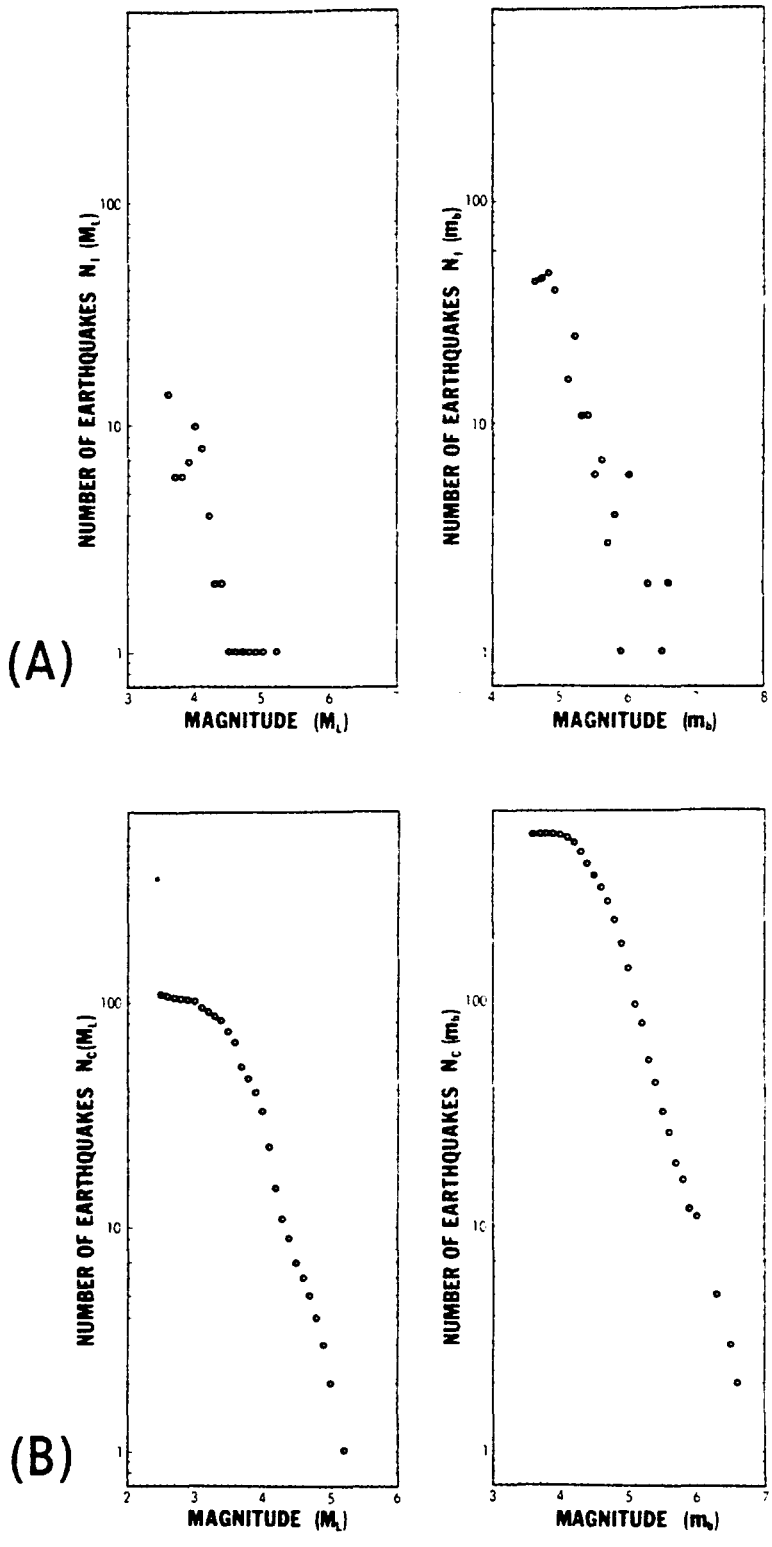

Figure 9. (A) Incremental magnitude distribution for aftershocks (left); shallow seismic belt (right). (B) Cumulative distribution of magnitudes for aftershocks (left); shallow seismic belt (right).

Administration (Meyers and von Hake, 1976). The sample covers the time period of April 1963 to May 1975. It includes 559 earthquakes located in a zone between the Peru-Chile trench axis and the Andean front and extends from 3°S to 18°S latitude.

The values of b computed for both the aftershock zone and shallow seismic belt (Table 7) are remarkably similar and bear a close resemblance with the established median of 0.8 to 0.9 generally observed for aftershock sequences and normal seismicity. The fact that the value of b for the aftershock zone is based on coda-length magnitudes supports the accuracy of these M_L estimates. There is also excellent agreement with the least squares computed values of 0.87 and 0.95 determined from incremental data by Deza (1970) for western South America between 0° and 26°S latitude. Evernden's (1970) b value of 1.11 for central South America (1966-1967) may reflect the use of cumulative data and a mixture of earthquakes from different seismic regimes.

STRESS DROP CONSIDERATIONS

The combined horizontal and vertical distribution of aftershocks imply an effective fault radius of approximately 100 kilometers. Assuming that the fault plane is circular (Keilis Borok, 1959) and that $M_S \simeq M_L$, Randall's (1973) graphical relationship between magnitude and effective fault radius leads to an estimated stress drop for the main shock of about 18 bars. This is consistent with the range of values obtained by Max Wyss (personal communication) for shallow underthrust earthquakes in the southwest and eastern Pacific. Moreover, Kanamori and Anderson (1975) show that, for 24 large shallow-focus inter-plate earthquakes, i.e., earthquakes located along plate boundaries, the stress drops range between 10 and 100 bars and have an average value of approximately 30 bars. The lower value of 18 bars, although well within the expected limits, may result, in part, from the unusually shallow depth of focus for a Peruvian inter-plate earthquake (Wyss, 1970).

Abe (1972), using an analytical method which relates stress drop to seismic moment (e.g., Kanamori and Anderson, 1975), computed a stress drop value which approaches 42 bars for the Peru earthquake of October 17, 1966 (M_S = 7.6, h = 38 kilometers). This earthquake occurred roughly 200 kilometers northwest of Lima and had a similar low-angle thrust fault mechanism (Abe, 1972). Applying Randall's (1973) technique to the 1966 earthquake results in an estimated stress drop of about 40 bars which is equivalent to Abe's solution. The close correspondence between these two values lends some support to the use

of Randall's graphical technique for this region in the case of the 1974 main shock.

DISCUSSION AND CONCLUSIONS

The Peruvian earthquake of October 3, 1974, is interpreted to have occurred in response to differential motion near the boundary separating an oceanic and a continental lithospheric plate. Large-magnitude earthquakes are frequently observed along such major plate boundaries and, when associated with island-arc structures such as the Peru-Chile trench, are normally located on the landward side of the trench axis. Kelleher (1972) has defined various seismic gaps within the shallow seismic zone of western South America based on "large" earthquakes during the past 60 years. The above investigation leads to one of the more interesting aspects of the 1974 earthquake in that the main shock and aftershock zone fill a seismic gap identified by Kelleher (1972) as a region of "relatively high earthquake risk." Also, Brady (1976) has suggested that the region of study is a possible source area for a magnitude-8+ earthquake within the next 4 to 12 years. In view of Brady's prediction, a thorough study of this earthquake assumes an even greater importance. The results obtained from the regional aftershock study coupled with the tectonic implications discussed by Spence et al. (1976), the intensity report of Espinosa et al. (1976), and the damage survey of Husid et al. (1976) constitute the most comprehensive seismological investigation of a South American earthquake to date.

From an assessment of the aftershock data, the following observations and conclusions are made:

1. Locations of 113 epicenters describe an irregular shaped zone approximately 210 kilometers long by 150 kilometers wide. The oceanward or long side trends south-southeast, subparallel to the coast. A dense cluster of aftershocks in the vicinity of Chilca suggests a higher degree of energy release for that area than elsewhere throughout the region.

2. The hypocentral distribution is compatible with shallow underthrusting and appears to delineate a zone (or slab) that may be as much as 40 kilometers thick. Inferred dip is between about 15° and 23°. Thickness of the zone could be somewhat less because of possible errors in the computed focal depths. Defining aftershock volume as the aftershock area (Figure 2) multiplied by the depth range of occurrence (Figure 5) give values within the limits of about 5 to 9 x 10^5 km^3.

3. Focal mechanisms are consistent with low-angle thrust faulting beneath the continental plate. If the strike and dip of the preferred B-plane of the main shock focal mechanism is assumed, the nodal plane projects through the hypocenter of the largest aftershock and also appears to form an upper bound to the majority of aftershock hypocenters (Figure 5).

4. Differences in location between the teleseismic and regional epicenters for the oceanward events indicates a general northerly bias of 10 to 20 km where the teleseismic location is toward the north. The east-west bias noted for the more coastal locations is, for the most part, due to variations in depth.

5. The distributions of magnitudes within the shallow seismic belt as well as the aftershock zone are nearly equivalent and imply a regional b value of approximately 0.90.

6. Estimation of the stress drop for the main shock based on magnitude and effective fault radius is 18 bars.

REFERENCES

Abe, K. (1972). Mechanisms and tectonic implications of the 1966 and 1970 Peru earthquakes, Phys. Earth Planet. Interiors 5, 367-379.

Algermissen, S. T., J. W. Dewey, C. J. Langer, and W. H. Dillinger (1974). The Managua, Nicaragua, earthquake of December 23, 1972: location, focal mechanism, and intensity distribution, Bull. Seism. Soc. Am. 64, 993-1004.

Bellido, B., E. (1969). Sinopsis de la geologia del Peru, Republica del Peru, Ministerio de Energia y Minas, Servico de Geologia y Mineria 22, 54 pp.

Bellido B., E. and L. de Montrenil D. (1972). Aspectos generales de la metalogenia del Peru, Republica del Peru, Ministerio de Energia y Minas, Servico de Geologia y Mineria, Geologia Economica No. 1, 149 pp.

Bolt, B. A. (1960). Earthquake epicenters, focal depths, and origin using a high-speed computer, Geoph. J. 3, 433-440.

Brady, B. T. (1976). Theory of earthquakes-IV. General implications of earthquake prediction, Pure Appl. Geoph. (in press).

Cisternas, A. (1964). Precision determination of focal depths and epicenters of earthquakes, CIT Publication, AFOSR Contract No. AF-49(638), 1337.

Deza, E. (1970). Zonas de transicion seismotectonica en Sudamerica estudio preliminar de la zona de transicion en el Peru, in Symposium on the Results of Upper Mantle Investigations with Emphasis on Latin America, Buenos Aires, Argentina, 143-156.

Draper, N. R. and H. Smith (1966). Applied regression analysis, John Wiley and Sons, 407 pp.

Engdahl, E. R. and R. H. Gunst (1966). Use of a high-speed computer for the preliminary determination of earthquake hypocenters, Bull. Seism. Soc. Am. 6, 325-336.

Espinosa, A. F., R. Husid, S. T. Algermissen, and J. de las Casas (1976). The Lima earthquake of October 3, 1974, intensity distribution, Bull. Seism. Soc. Am. (in press).

Evernden, J. F. (1970). Study of regional seismicity and associated problems, Bull. Seism. Soc. Am. 60, 393-446.

Dillinger, W. H., S. T. Harding, and A. J. Pope (1972). Determining maximum likelihood body wave focal plane solutions, Geoph. J. 30, 315-329.

Geiger, L. (1910). Herdbestimmung bei Erdbeben aus den Ankunftszeiten, K. Gesen. Wiss. Gott 4, 331-349.

Gutenberg, B. and C. F. Richter (1954). Seismicity of the Earth and Associated Phenomena, 2nd ed., Princeton Univ. Press, 310 pp.

Hayes, D. E. (1966). A geophysical investigation of the Peru-Chile trench, Marine Geology 4, 309-351.

Hayes, D. E. (1974). Continental margin of western South America, in The Geology of Continental Margins, edited by C. A. Burk and C. L. Drake, Springer-Verlag New York Inc., 581-590.

Husid, R., A. F. Espinosa, and J. de las Casas (1976). The Lima earthquake of October 3, 1974, damage distribution, Bull. Seism. Soc. Am. (in press).

Hussong, D. M. (1972). Detailed structural interpretation of the Pacific Ocean crust using ASPER and ocean bottom seismometers, Ph.D. Thesis, Univ. of Hawaii, Honolulu, Hawaii, 165 pp.

Hussong, D. M., P. B. Edwards, S. H. Johnson, J. F. Campbell, and G. H. Sutton (1976). Crustal structure of the Peru-Chile trench: 8°-12°S latitude in The Geophysics of the Pacific Ocean Basin and its Margin, Geophysical Monograph 19, edited by G. H. Sutton, M. H. Maughnani and R. Moberly, American Geophysical Union, Washington, D.C., 71-85.

Isacks, B., J. Oliver, and L. Sykes (1968). Seismology and the new global tectonics, J. Geoph. Res. 73, 5855-5899.

Isacks, B. and P. Molnar (1971). Distribution of stresses in the descending lithosophere from a global survey of focal-mechanism solutions of mantle earthquakes, Rev. Geoph. Space Phys., 9, 103-174.

James, D. E., I. S. Sacks, E. Lazo L., and P. Aparicio G. (1969). On locating local earthquakes using small networks, Bull. Seism. Soc. Am. 59, 1201-1212.

Jenks, W. F. (1956). Peru, in Handbook of South American Geology, Geol. Soc. Am., Memoir 65, 215-247.

Johnson, S. H., G. G. Connard, C. M. Hussong, and G. E. Ness (1973). Crustal structure of the north central Nazca plate, paper presented at the Geodynamics Symposium, XVIIth meeting, Int. Assoc. of Seism. and Phys. of the Earth's Interior, Lima, Peru.

Kanamori, H. and D. L. Anderson (1975). Theoretical basis of some empirical relations in seismology, Bull. Seism. Soc. Am., 65, 1073-1095.

Karnik, V. (1971). Seismicity of the European Area Part 2, D. Reidal Publishing Co., Dordrecht, Holland, 218 pp.

Karnik, V. and D. Prochazkova (1971). Problems of Determination of the magnitude-frequency relation, Studia Geoph. et Geod. 15, 95-99.

Lee, W. H. K. and J. C. Lahr (1975). HYP071 (revised): A computer program for determining hypocenter, magnitude, and first-motion pattern of local earthquakes, U.S. Geol. Survey Open File Report 75-311, 113 pp.

Lee, W. H. K., R. E. Bennet, and K. L. Meagher (1972). A method of estimating magnitude of local earthquakes from signal duration, U.S. Geol. Survey Open File Report, 28 pp.

Ocola, L. C. and R. P. Meyer (1973). Crustal structure from the Pacific Basin to the Brazilian Shield between 12° and 30° south latitude, Bull. Geol. Soc. Am. 84, 3387-3404.

Meyers, H. and G. A. von Hake (1976). Earthquake Data File Summary, U.S. Dept. of Commerce, NOAA, Environmental Data Service, National Geophysical and Solar-Terrestrial Data Center, Boulder, Colorado, 32 pp.

Page, R. (1968). Aftershocks and microaftershocks of the great Alaska earthquake of 1964, Bull. Seism. Soc. Am. 58, 1131-1168.

National Oceanic and Atmospheric Administration (1973). Preliminary determination of epicenters, EDR 76-72, National Earthquake Information Center, National Oceanic and Atmospheric Administration, Boulder, Colorado, 18-20.

Randall, M. J. (1973). The spectral theory of seismic sources, Bull. Seism. Soc. Am., 63, 1133-1144.

Richter, C. F. (1958). Elementary Seismology, W. H. Freeman and Co., San Francisco, California.

Silgado, E. (1968). Historia de los seismos mas notables occurridos en el Peru (1513-1960), Bol. Bibliogr. Geofis. Oceanogr. Amer. 4, 193.

Silgado, E. (1973). Historia de los seismos mas notables occurridos en el Peru (1555-1970), Geofisica Panamerica 2, 179-243.

Spence, W., C. J. Langer, and J. N. Jordan (1976). A tectonic study of the Peru earthquakes of October 3 and November 9, 1974, Bull. Seism. Soc. Am. (in preparation).

Stauder, W. (1975). Subduction of the Nazca plate under Peru as evidenced by focal mechanisms and by seismicity, J. Geoph. Res. 80, 1058-1064.

U.S. Geological Survey (1974a). Preliminary determination of epicenters monthly listing, September, 1974, National Earthquake Information Service, USGS, Golden, Colorado, 8 pp.

U.S. Geological Survey (1974b). Preliminary determination of epicenters monthly listing, October, 1974, National Earthquake Information Service, USGS, Golden, Colorado, 11 pp.

U.S. Geological Survey (1974c). Preliminary determination of epicenters monthly listing, November, 1974, National Earthquake Information Service, USGS, Golden, Colorado, 8 pp.

Utsu, T. (1967). Some problems of the frequency distribution of earthquakes in respect to magnitude, Geoph. Bull. Hokkaido Univ., 17, 53.

Wagner, D. (1972). Statistical decision theory applied to the focal mechanisms of Peruvian earthquakes, Ph.D. Thesis, St. Louis Univ., St. Louis, Missouri, 176 pp.

Woollard, G. P. (1975). The interrelationships of crustal and upper mantle parameter values in the Pacific, Rev. of Geoph. 14, 87-137.

Wyss, M. (1970). Stress estimates for South American shallow and deep earthquakes, J. Geoph. Res. 75, 1529-1544.

The vita has been removed from the scanned document

ABSTRACT

Locations of 113 aftershocks of the magnitude-7.6 (M_S) Peruvian earthquake of October 3, 1974, were determined from data obtained by a ten-station network installed along the coastal area between lat 11° and 14° S. These epicenters define an irregular shaped zone approximately 210 km long by 150 km wide, the oceanward or long side of which trends subparallel with the coast and extends between about lat 12° and 13.8° S. The distribution of hypocenters ranges in depth from near surface to roughly 65 km and is indicative of shallow underthrusting. Focal mechanisms are consistent with low angle thrust faulting. A b value of approximately 0.90 was determined for earthquakes within the Peruvian shallow seismic belt (1963-1975) and the aftershock sequence.